IEEE Access
Multidisciplinary | Rapid Review | Open Access Journal

Date of publication xxxx 00, 0000, date of current version xxxx 00, 0000.

Digital Object Identifier 10.1109/ACCESS.2024.Doi Number

Polypropylene's crystallization morphology during the non-isothermal crystallization process and its electrical properties

Wei Wang[1], Wanting Jiang[2], Lin Yan[3], Dongdong Yang[1] and Fengjie MA[4]

[1]State Grid Shanxi Electric Power Research Institute, Taiyuan 030012, China
[2]State Grid Linfen Power Supply Company, Linfen 041000, China
[3]State Grid Taiyuan Power Supply Company, Taiyuan 030000, China
[4]International Institute of Engineering, Changsha University of Science & Technology, Changsha 410004, China

Corresponding author: Wei Wang (e-mail: 604186127@qq.com).

This work was supported in part by the Science and technology project of State Grid Shanxi Electric Power Co., Ltd. under Grant 52053023000G, 520530202002 and 52053020000Y."

ABSTRACT To understand the mechanism of the effect of the cooling rate of the non-isothermal crystallization process on the crystallization morphology of polypropylene (PP) insulation, and the relationship between the crystallization morphology and DC breakdown performance, this paper researched the crystallization morphology, physicochemical property, polarization current and DC breakdown strength of PP specimens with five cooling rates. As the cooling rate increases, due to the reduction of the diameter and perfection degree of PP spherulites, the density of amorphous regions increases, deep traps are introduced, and the DC breakdown strength is enhanced. The DC breakdown strength of PP specimen with a cooling rate of 170 °C/min is about 2.4 times higher than that of PP specimen with a cooling rate of 10 °C/min. Therefore, by controlling the cooling rates, the crystallization regulation of PP can be realized. That is, by affecting the development process of PP nucleation and spherulites development, resulting in changes in the crystallization morphology, which in turn changes the properties of PP such as glass transition temperature, melting range, and breaking elongation. Finally, the regulation of carrier transport in PP, i.e., insulation properties, is realized, which provides a basis for the improvement of PP insulating materials.

INDEX TERMS Polypropylene; cooling rate; crystalline morphology; electrical properties

I. INTRODUCTION

High voltage direct current (HVDC) transmission has inherent advantages in long-distance power delivery with lower losses and is a major trend toward the future development of power grids [1–3]. Compared to overhead lines, DC power cables are considered the only option for a number of circumstances, such as offshore wind export lines, island power supply, and long-distance transmission across the sea when a DC connection is desired [4]. However, the requirement of the surrounding insulations limits the operating voltage levels of power cables, and heat dissipation is an issue for conductor cores enclosed in polymer insulations with comparatively low thermal conductivities. Compared with crosslinked polyethylene (XLPE), one of the traditional cable insulation materials, PP has more excellent heat resistance and electrical properties, which is important to enhance the cable load capacity and voltage level. Crosslinked polyethylene (XLPE) is a widely used polymer insulation material for power cables, with a maximum running temperature of 90°C per IEC 60502, which restricts the further development of XLPE cables to meet the increasing demands of the voltage level and transmission capacity. Polypropylene-based HVDC cables are an emerging technology and have been extensively studied in recent years. The higher melting point of PP (up to 165 °C) and excellent dielectric performance make PP cables potentially operate at a much higher temperature, thus achieving an elevated transmission capacity [5,6,7].

Polypropylene is a typical semi-crystalline material where the crystal regions are formed with regularly arranged polymer chains and usually develop spherulites

with decreasing crystallinity from cores (nuclei) to the edges. Surrounding regions that have a disordered chain arrangement is the so-called amorphous phase. Mechanical and dielectric properties of PP could be greatly related to crystal structures and their aggregate states within the amorphous matrix. [8,9]. These morphological properties of PP could be affected by many factors during the manufacturing process, such as thermal history, applied stress, and additives [10]. From the perspective of crystallization kinetics, the PP's crystallization process is divided into two categories: isothermal crystallization and non-isothermal crystallization. Isothermal crystallization is a crystallization process under constant temperature conditions. In the manufacturing process of polymer-insulated power cables, the insulation layer is extruded at high temperatures after hot melting by a non-isothermal crystallization process. Therefore, it is not only of theoretical significance but also of significant engineering value to study the relationship between non-isothermal crystallization form and insulation performance of PP.

In 1968, Kolesov S N et al. found for the first time that the AC breakdown strength of PP increases with decreasing spherulite diameter. In 1980, this team obtained PP spherulite from 5 to 145 μm by heat treatment, measured the breakdown strength of spherulite and inter-spherulitic space (ISS) separately, and found that the breakdown strength of spherulite was higher [11]. Also, the variation in the size of the spherulites will have an effect on the crystallinity. Kazuo I obtained PP films with different crystallinity from 50% to 80% by heat treatment and found that the ionic jump distance depends mainly on the crystallinity of the polymer [12]. It can be seen that different crystallization morphology affects the insulating properties of PP. Therefore, the researchers adjusted the crystallization of PP by heat treatment to obtain PP specimens with different crystalline morphologies. Commonly used heat treatments include liquid nitrogen [13], water bath[14], oil bath[15], and air cooling[16].

Zheng F et al. prepared PP specimens in two crystalline forms: one by slow cooling by clamping in an iron plate at 60°C and the other by rapid cooling by placing in liquid nitrogen. It was concluded that the amorphous region is the main factor affecting the breakdown field strength [13]. Zhang L et al. prepared three PP specimens with fast, medium, and slow cooling rates in an ice-water bath, air, and a high-temperature drying oven, respectively. The results show that the electrical properties of the well-dispersed β-crystalline PP system under a high external field are comprehensively improved [17]. Li Z comparatively studied both non-isothermal and isothermal crystallization. Three non-isothermal crystallization cooling rates of 10 °C/min, 5 °C/min, and 2.5 °C/min were set. Two isothermal crystallization temperatures at 128°C and 132°C were set. The reduction of the spherulite size limits the development of an electrical tree in the amorphous region at the spherulite interface [18]. The above study helps to understand the effect of non-isothermal crystalline morphology related to the cooling rate on the insulation properties of PP. However, these studies provide a sketchy description of the heat treatment process and lack a quantitative analysis of the cooling rate. There are also studies that design only 2 or 3 cooling rates, which failed to comprehensively study the crystallization morphology at each non-isothermal crystallization cooling rate.

In this paper, the cooling rate of a non-isothermal crystallization process is used as the only variable, and a novel method is proposed that enables process control of the cooling rate: an experimental setup was designed to realize the regulation of the cooling rate, and five cooling rates were set between slow cooling and air cooling. The process is described in detail below. On this basis, the physical, mechanical, and electrical properties of the specimens with different crystallization morphologies obtained by heat treatment were tested. According to the test results, the effect of cooling rate on the crystallization morphology of polypropylene was analyzed, and the mechanism of the effect of crystallization morphology on the DC breakdown characteristics of polypropylene was investigated by combining the carrier transport characteristics and trap characteristics of the specimens.

II. EXPERIMENTAL SETUP

A. SPECIMEN PREPARATION

In this paper, PP specimens with different thermal history were prepared by controlling the cooling rate of PP after hot press molding. The specimen preparation process is shown in Figure 1. Firstly, the PP pellets (Yangzi Petrochemical, PPH-T03-S-F401) were pretreated in an electric drying oven at 60°C for 12 h to remove the moisture from the raw material. Then the pretreated PP raw material was placed in a mold. After preheated at 200°C for 5 min in a hot press machine, PP was hot pressed at 15 MPa for 5 min. Finally, the outermost molds were removed or retained, and the rest part was immediately placed in a drying oven with different temperatures. After the temperature of the mold was reduced to about 90°C, the mold was removed from the drying oven and cooled to room temperature. The thickness of the PP film is about 200 μm.

The process of controlling the cooling rate is as follows. After the hot pressing was finished, the mold was put into the electric drying oven with the temperature T_{set}, at which time the mold temperature was the starting temperature T_0. The duration for the mold temperature to drop to the end temperature T_1 (about 90°C) was t_s. During the cooling process, the pyrometer records the mold temperature T once per second. 5 groups of data were tested at each cooling rate, and a graph of the relationship between the mold temperature T and time t during the cooling process was

obtained, as shown in Figure 2, satisfying the following function:

$$T = ae^{-\frac{t}{b}} + c \tag{1}$$

where a, b, and c are constants.

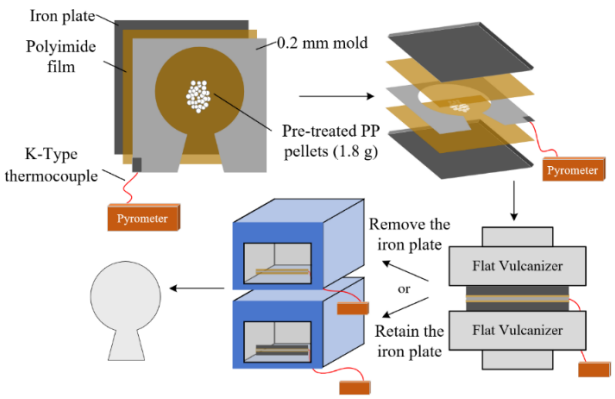

FIGURE 1. **Specimen preparation process.**

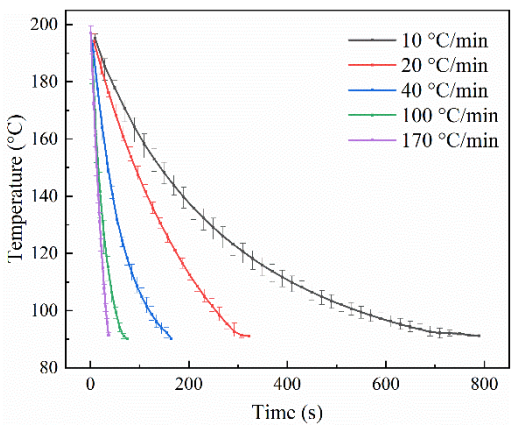

FIGURE 2. **Mold cooling temperature.**

The average cooling rate of the mold $V_m=(T_0-T_1)/t_s$ was taken as the approximate cooling rate of the PP in this study. The temperature control error of the drying oven is ±1°C. The temperature measurement with a K-type thermocouple has an error of ±0.5°C. The accuracy of the thermocouple pyrometer is ±(0.5%rdg+1) °C, the temperature sampling rate is 2.5 times per second, and the resolution is 0.1°C.

Pure PP specimens with a cooling rate of 10 °C/min ~ 200 °C/min were prepared by the above method. Pre-experiments were done on these specimens to observe their crystalline morphology and the five most representative specimens were selected. The details of the five specimens are listed in Table I.

B. CHARACTERIZATION

1) CRYSTALLINE MORPHOLOGY OBSERVATION

A Leica DM2500M microscope was used to observe the non-isothermal crystallization process of PP. A 2 cm × 2 cm sheet was cut from a 200 μm specimen and placed on a silver hot plate that has an error of ±0.1°C. It was first heated to 200°C and then held for 5 min to eliminate the influence of the thermal history. The specimen was then cooled from 200 °C to 90 °C at a rate of 10 °C/min, and the crystallization process was recorded with images taken per 1 s.

TABLE I
INDEX FOR PP SPECIMENS

Index	Specimen preparation condition	Cooling rate
PP-1	T_{set}=90°C, retain the iron plate	10±2 °C/min
PP-2	T_{set}=65°C, retain the iron plate	20±2 °C/min
PP-3	T_{set}=30°C, retain the iron plate	40±3 °C/min
PP-4	T_{set}=70°C, remove the iron plate	100±4 °C/min
PP-5	T_{set}=30°C, remove the iron plate	170±4 °C/min
PP-5	T_{set}=30°C, remove the iron plate	170±4 °C/min

2) MELTING TEMPERATURE AND CRYSTALLINITY MEASUREMENT

Differential scanning calorimetry (DSC) analysis is conducted by investigating the melting and crystallization behavior of PP specimens by a NETZSCH STA 449F5. Melting curves were obtained by heating approximately 8 mg of PP specimens from 30°C to 250°C under an argon atmosphere with a gas flow rate of 60 mL/min. The specimen was then held at 250°C for 15 min and cooled to 30°C subsequently at a rate of 10 °C/min to obtain the crystallization curve. The starting of melting temperature, melting range, and crystallinity of the PP specimens obtained from melting curves are defined as follow. The starting of melting temperature is the temperature corresponding to the starting point of the melting peak. The melting range is the temperature corresponding to the end of the melting peak minus the starting of melting temperature. The crystallinity X_c is calculated by:

$$X_c = \frac{\Delta H_m}{\Delta H_r} \tag{2}$$

where ΔH_m is the melting enthalpy of PP specimens, and its value is obtained by estimating the area of the melting peak; ΔH_r is the melting enthalpy for PP with 100% crystallinity, and ΔH_r = 209 J/g is used here.

3) DYNAMIC MECHANICAL ANALYSIS

Dynamic mechanical analysis (DMA) was performed on PP specimens using a NETZSCH DMA 242, where storage modulus E', and loss modulus E'' were measured. The loss factor tgδ was obtained as follows equation:

$$\mathrm{tg}\delta = \frac{E''}{E'} \tag{3}$$

E' characterizes the material's ability to resist deformation, and the higher the E' of the material, the stronger its ability to resist deformation. E'' describes the viscosity of the material. tgδ characterizes the damping of the material. The tensile mode was selected during the DMA test, with a dynamic force applied (1 Hz, 3.618 N) in a temperature range from −100°C to 150°C.

4) TENSILE TEST

Quasi-static tensile tests were performed on an Instron 3344 universal testing system with a fixed speed of 50 mm/min at room temperature. Dumbbell-shaped specimens used for the tests are shown in Figure 3 with a thickness of 0.2 mm. The gauge length is 20 mm. The breaking elongation, tensile strength, and elastic modulus were obtained from the stress-strain curves. The specimens were tested five times at each cooling rate and the average value was taken as the test result.

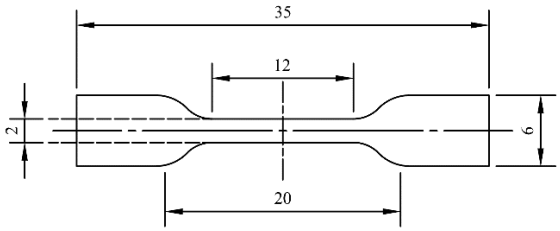

FIGURE 3. **Dumbbell-shaped specimens (unit: mm).**

There are three groups of words that describe the mechanical properties of materials as follows: brittle and tough, strong and weak, and hard and soft. Their combination provides a more complete description of the mechanical properties of a material, such as a material that is hard and brittle. These words correspond to the characteristic quantities that characterize mechanical properties. For example, the elastic modulus primarily describes the soft and hard properties of a material. It is important to note that there is not a one-to-one correspondence between characteristic quantities and properties. For example, the elastic modulus can to some extent also characterize the strong and weak properties of a material. In summary, the evaluation of the mechanical properties of materials should be combined with multiple characteristic quantities for comprehensive description. In this paper, a coordinate system is established as shown in Figure 4. For ease of description, the characteristic quantities are here corresponded to their main described properties. It is considered that the larger the elastic modulus the harder the material, the larger the tensile strength the stronger the material, and the larger the breaking elongation the tougher the material.

5) SPACE CHARGE MEASUREMENT

The space charge distribution in the specimens was measured by a Peanuts space charge measuring system from FiveLab Co., Ltd. based on the pulse electro-acoustic (PEA) technique. The bottom electrode is an aluminum plate. The upper electrode is semiconductor material. Silicone oil is applied to both sides of each specimen of 200 μm thickness to avoid surface and corona discharges during polarization. During measurement, the specimen was polarized at 40 kV/mm for 60 min and then depolarized for 30 min after removing of the high voltage. Tests are performed at room temperature. The pulse voltage frequency is 400 Hz with an amplitude is 200 V.

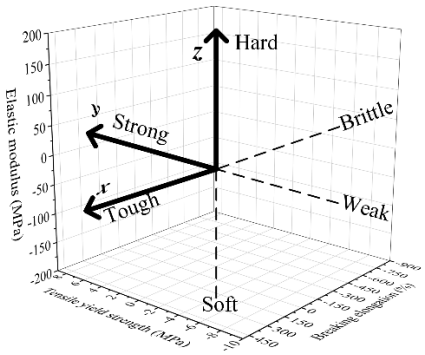

FIGURE 4. **Three-dimensional coordinate system for describing mechanical properties.**

6) POLARIZATION CURRENT MEASUREMENT

The polarization currents in PP specimens under different DC voltages were measured using circular electrodes with a guard ring. The diameters of the upper and lower electrodes are 40 mm and 25 mm, respectively. The width of the guard ring electrode is 5 mm. The thickness of the specimen was 200 μm and the diameter was 50 mm. The applied electric field is ranging from 5 kV/mm to 45 kV/mm, with an interval of 5 kV/mm. The duration of each measurement is 20 min. Before each measurement, the specimen was grounded for 15 min to release the bulk charge.

7) DC BREAKDOWN STRENGTH

The DC breakdown strength of PP specimens was measured by placing film specimens between ball electrodes. The diameter of the copper ball electrode is 20 mm. The testing region was immersed in silicone oil during the measurement to avoid the happening of surface flashover. The applied voltage was increased at a rate of 1 kV/s until breakdown occurs. At least 15 tests for each type of PP. Weibull probability plot is adopted here to present the obtained data in which probability P of breakdown can be expressed as:

$$P = 1 - \exp\left[-\left(\frac{E_i}{\alpha_s}\right)^{\beta_s}\right] \tag{4}$$

$$P_i = \frac{i - 0.44}{n + 0.25} \times 100\% \tag{5}$$

Where P is the cumulative breakdown probability, representing the cumulative possibility density distribution of specimen breakdown; E is the breakdown field strength; β_s is a shape parameter, and the larger the value is, the smaller the data distribution is; α_s is the scale parameter, which represents the breakdown field strength when the cumulative probability value P is 63.2%. i is the i-th value after sorting E from smallest to largest; n is the total number of test points.

III. EXPERIMENT RESULT

A. CRYSTALLINE MORPHOLOGY

Figure 5 shows the crystallization process of PP at a cooling rate of 10 °C/min with two distinguishable stages, namely

nucleation and spherulite growth stage [19]. The nucleation stage is shown in Figure 5a. When the temperature drops to about 129.7°C, a number of nuclei can be seen in PP melts, while some nuclei formed even earlier have developed into tiny spherulites. As the temperature continues to decrease, the spherulite growth stage begins. As shown in Figure 5b and 5c, the diameter of the spherulites is increasing, and the adjacent spherulites are squeezing each other to form ball crystal boundaries. After the PP cools to about 116.7°C where no obvious morphology change can be observed as shown in Figure 5d, the existence of non-crystal region, amorphous regions, can be seen between spherulites.

Figure 6 shows the crystalline morphology of PP with different cooling rates. With the increase of the average cooling rates, the diameter of the spherulites keeps decreasing. The spherulites structure of PP-1 is clearly visible. With the increase of the cooling rate of heat treatment, the morphology and grain boundaries become blurred.

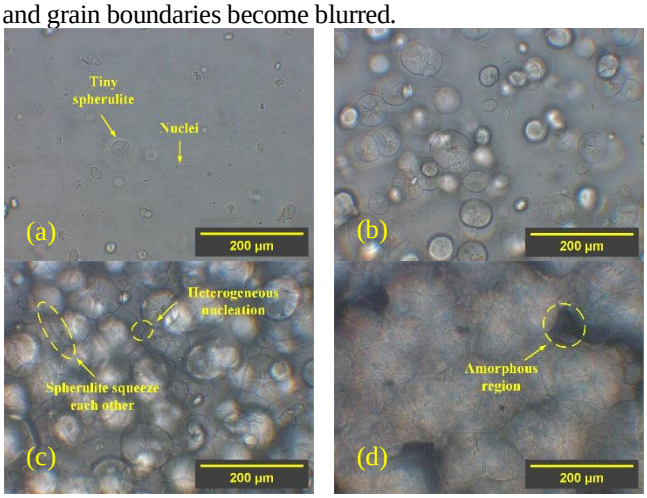

FIGURE 5. **PP crystallization process at 10 °C/min cooling rate. (a) 129.7°C, (b) 125.7°C, (c)123.3°C, (d)116.7°C.**

B. CRYSTALLIZATION AND MELTING CURVE

Figure 7 shows the crystallization curve of the PP specimens. The crystallization process continues when the temperature is reduced to about 116.7°C, but it is no longer possible to observe the evident crystallization process via a microscope, as shown in Figure 5d. The crystallization ends when the temperature drops to about 90°C. Therefore, in this paper, the ending temperature T_1 is taken as 90°C when calculating the average cooling rate.

Three features, melting range ΔT, starting of melting temperature T_s, and crystallinity X_c, were extracted from the melting curve. Their relationship with cooling rate is shown in Figure 8. ΔT and T_s can characterize the degree of crystalline perfection, and imperfect crystals will melt at a lower temperature and have a wider melting range [16,20,21]. PP-1 has the highest T_s and the shortest ΔT; PP-5 has the lowest T_s and the longest ΔT. This indicates that the large spherulites of PP-1 are more perfect than the small spherulites of PP-5. Also PP-1 and PP-5 have the same X_c of 33%. The cooling rates of PP-2, PP-3, and PP-4 increase sequentially, their T_s increase and then decrease, and ΔT decreases and then increases. This indicates that the degree of spherulites perfection of PP-2~PP-4 increases and then decreases. The X_c of PP-3 is the highest, 48%.

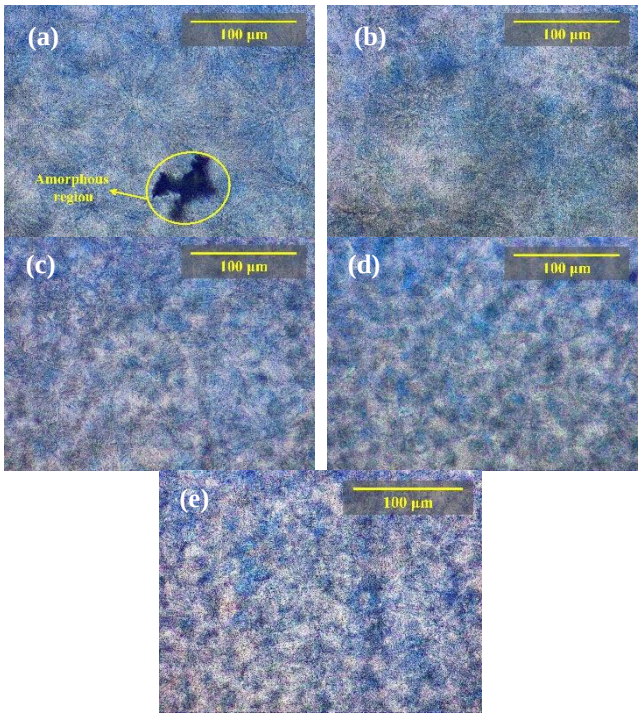

FIGURE 6. **Crystalline morphology of specimens at different cooling rates. (a) PP-1, (b) PP-2, (c)PP-3, (d)PP-4, (e)PP-5.**

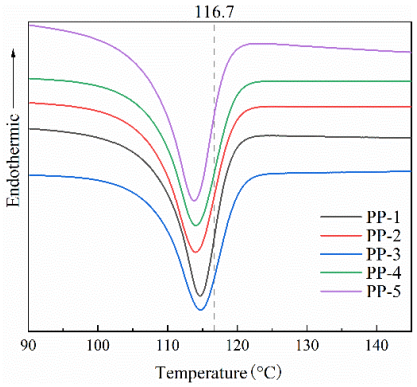

FIGURE 7. **Crystallization curve of PP specimens.**

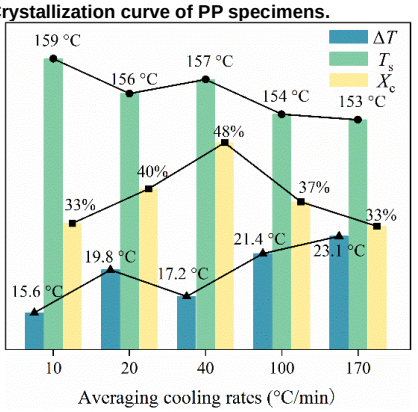

FIGURE 8. **Melting range, starting of melting temperature and crystallinity.**

C. DYNAMIC MECHANICAL ANALYSIS

Figure 9 shows the DMA test results of PP specimens in the range of −100°C ~ 150°C. As the Figure 9a shows, the storage modulus *E*' of all specimens decreases with the increase of temperature because the material gradually becomes softer and less rigid. Except for PP-2 and PP-3, which have a lower starting storage modulus, the difference in *E*' between the different specimens in the glass transition region is slight. Figure 9b shows that the tgδ of PP specimens have two relaxation peaks. The α peaks at high temperatures originates from the molecular motion in the crystalline region. The β peak near 10°C corresponds to the glass transition temperature T_g, the lowest temperature at which the molecular chain can move [22]. The glass transition temperatures of PP-1~PP-5 are shown in Table II. As can be seen from Table II, the T_g of PP-1 is lower than that of other specimens. It is shown that in slow-cooled PP-1 constraint of the amorphous region is weakened, and the force between spherulites is also weakened. Therefore, the transition from the glassy state to the highly elastic state occurs at a lower temperature. So the β peak of PP-1 is shifted towards lower temperature compared to other specimens.

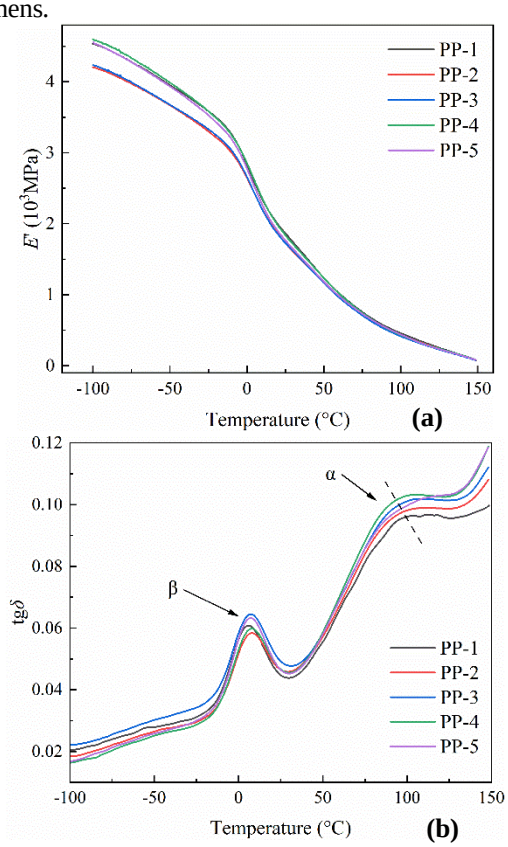

FIGURE 9. DMA test result. (a) *E*' and (b) tgδ of PP specimens

A. TENSILE TEST

The stress-strain curves of the PP specimens are reported in Figure 10. PP-1 shows great brittleness and breaks apart just at the end of the strain softening phase. The other 4 specimens showed small upward fluctuations in the plastic deformation stage. The values of the tensile strength σ_t, breaking elongation e_s, and elastic modulus E_s are listed in Table III. Calculate the mean value of each characteristic quantities in Table III. Subtract the mean value from the characteristic quantities and put the difference into the coordinate system of Figure 4 to obtain Figure 11. As shown in Figure 11, the quadrant where PP-1 is located indicates that it is brittle and hard relative to other specimens. It indicates that the molecular chains of PP-1 are weakly resistant to deformation, and the force between spherulites is reduced, which is consistent with the DMA test results. PP-2 and PP-3 are in the same quadrant and they are harder than the rest of the specimens. PP-4 and PP-5 are both below the *z*=0 plane and are softer and stronger than the rest of the specimens. Meanwhile, PP-5 is stronger than PP-4. This is due to the decrease in the size of the spherulites which favors the enhancement of the toughness of the material. Comparing all the parameters, PP-5, which is tough, strong, and soft, better meets the mechanical requirements for cable insulation. PP-5 not only has higher deformation and tensile resistance but is also easy to bend and not easily damaged.

TABLE II
GLASS TRANSITION TEMPERATURE OF PP SPECIMENS

Name	PP-1	PP-2	PP-3	PP-4	PP-5
T_g (°C)	5.7	8.0	7.6	8.1	7.6

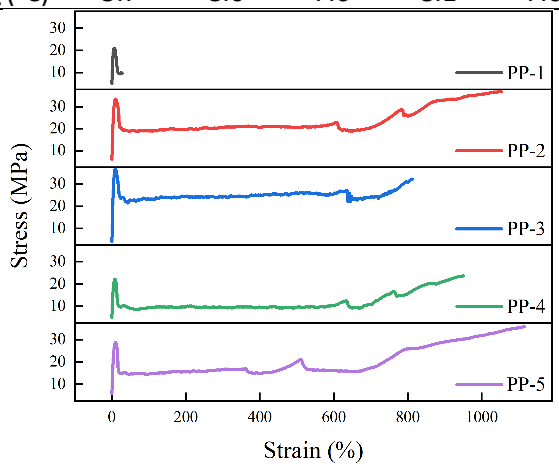

FIGURE 10. Tensile stress-strain curves of the PP copolymers

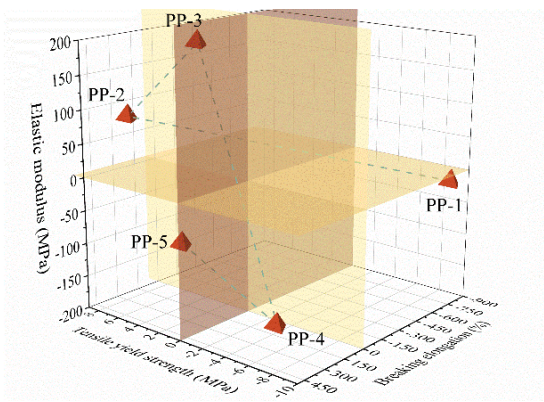

FIGURE 11. Three-dimensional coordinate diagrams characterizing mechanical properties

TABLE III
SUMMARY OF THE MECHANICAL PROPERTIES OF THE PP

Name	Breaking elongation (%)	Tensile strength (MPa)	Elastic modulus (MPa)
PP-1	19.2	20.2	665.0
PP-2	1050.4	37.8	758.1
PP-3	859.9	33.6	869.8
PP-4	990.8	25.0	500.0
PP-5	1077.2	32.4	590.1

B. POLARIZATION CURRENT

Figures 12a to 12e shows the polarization current of different PP specimens under DC voltage. PP-1 has a high and extremely unstable polarization current value at 35 kV/mm, so the polarization currents at 40 kV/mm and 45 kV/mm are not shown. As shown in the Figures, the polarization current decreases exponentially with the duration of specimens under DC field. Comparing the polarization currents of different specimens under the same voltage level, it can be found that the polarization currents of PP-1 are significantly higher than that of the other specimens. According to the analysis of DMA and DSC test results, the spherulite part of PP-1 is perfect, but the interspherical force is small. At the same time, the molecular chains in the amorphous region of PP-1 are loosely structured with small constraints. This is because boundary regions with higher impurities density that form conductive pathway that contribute to the large polarization current.

Comparing the polarization currents of the same specimen under different electric field strengths, it can be found that the polarization currents increase with the increase of electric field strength when the applied voltage time is the same. Under a lower electric field, no charge injection occurs, while impurities and polar groups polarize into carriers and migrate continuously along the direction of the electric field. In this condition, the conductive current inside the PP specimen is generally proportional to the field strength and satisfies Ohm's law. As the electric field strength increases, the charge injected by the electrode gradually plays a major role. The injected electrons continuously trap and de-trap, finally migrating deeper into the dielectric. At this time, the conductivity increases, the space charge in the insulation produces a space charge limited current (SCLC), and the conductive mechanism changes. The conductivity current i_{1200} at 1200 s of polarization is taken as the quasi-steady-state conductivity current of the specimen. The corresponding quasi-steady-state conductivity current density J is calculated from i_{1200} as:

$$J = \frac{i_{1200}}{S} \tag{6}$$

where S is the area of the measuring electrode.

In the double logarithmic coordinate system, a linear fit of J under the low and high field region is performed separately to obtain the lg$J$-lg$E$ curve, as shown in Figure 13f. The electric field strength corresponding to the point where the transition occurs in the low and high field regions is the threshold field strength E_{th} of the PP specimens. At the threshold field strength E_{th}, the conductive mechanism of PP is transformed. The variation of the E_{th} of PP-1 to PP-5 is reported in Table IV. It can be seen that the E_{th} is lower for the specimens with a slow cooling rate, which means that the polarization phenomenon of the slow-cooled specimens at low field strength is more evident.

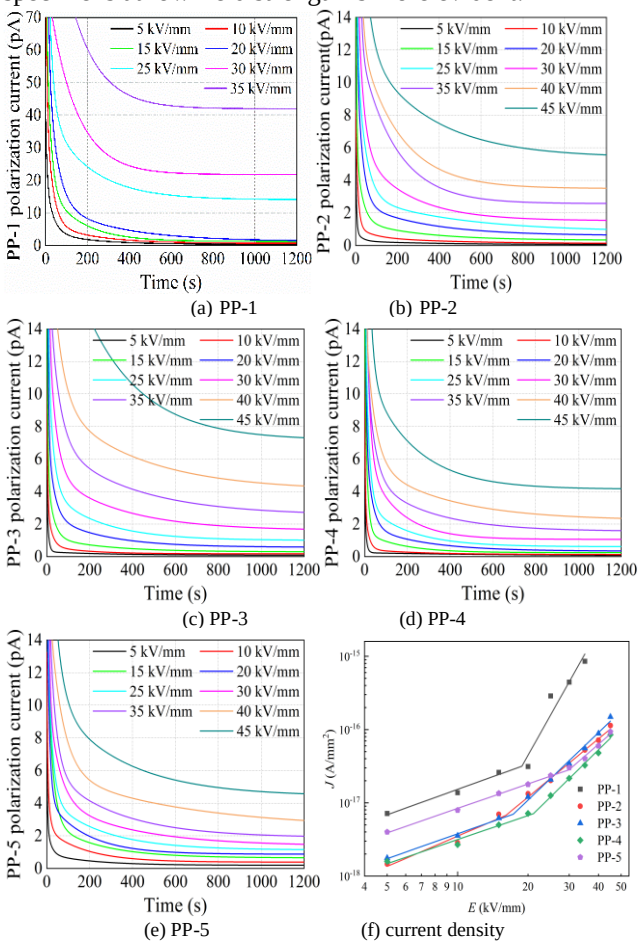

FIGURE 12. **Polarization current under different electrical field.**

TABLE IV
THRESHOLD FIELD STRENGTH FOR DIFFERENT SPECIMENS

Name	PP-1	PP-2	PP-3	PP-4	PP-5
E_{th} (kV/mm)	18.8	16.1	17.3	21.1	30.0

A. SPACE CHARGE MEASUREMENT RESULTS

Figure 13 shows the space charge curves of PP specimens polarized at 40 kV/mm for 60 min and depolarized for 30 min. From Figure 13(a) to 13(e), it can be seen that there is no heterocharge accumulation near the electrodes of all PP specimens. Except for PP-3, the cathodes of specimens

show homocharge injection, and the depth of injection increases with time.

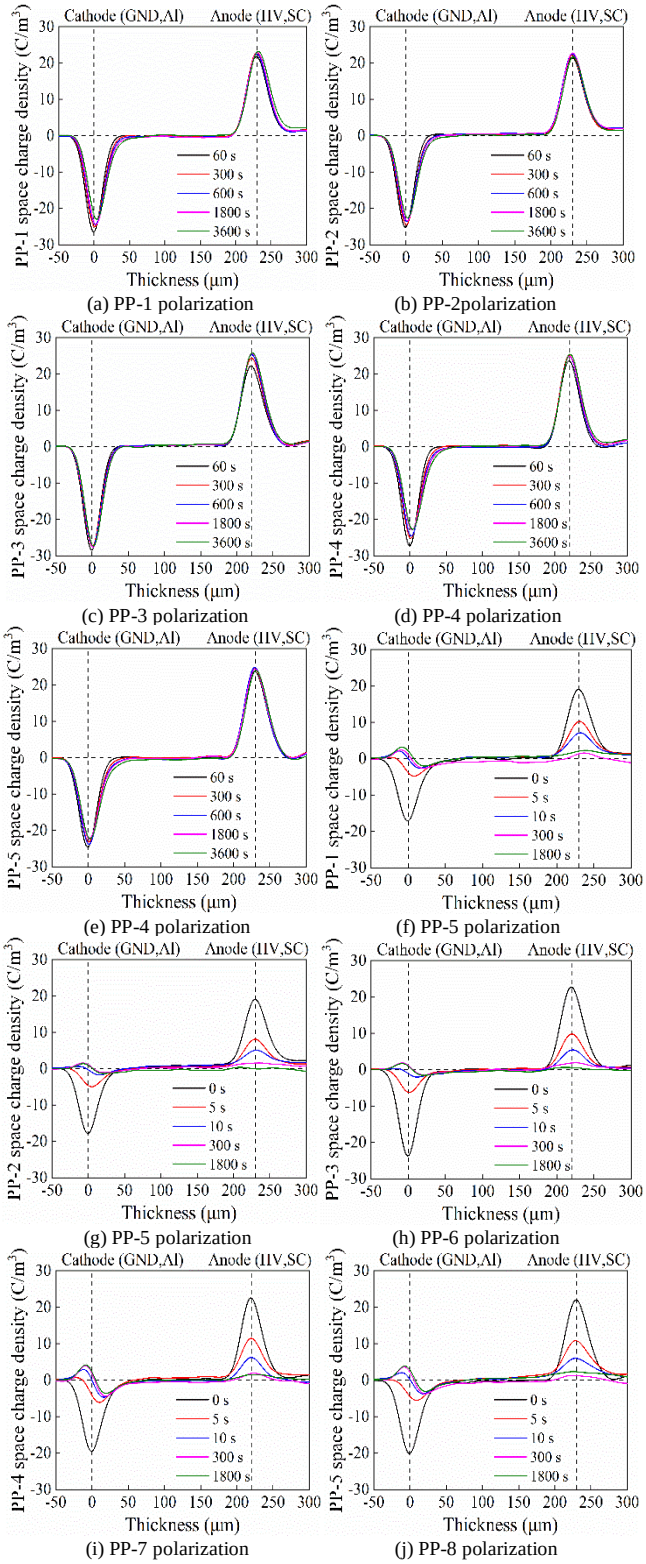

FIGURE 13. **Space charge measurement results.**

It can be seen from Figure 13(f) to 13(j) that during the depolarization process, there is an evident difference in the dissipation rate of the homocharge packet near the cathode for specimens with different cooling rates. There is almost no injection of homocharge in PP-3. Therefore, the charge decays rapidly to a smaller value during depolarization. The charge injection in both PP-4 and PP-5 specimens with higher cooling rates can be neglected at the anode, but the charge injects near the cathode in both cases, while the injection depth of the charge is deeper in PP-5. It can be concluded that crystalline morphology significantly affects the trap distribution of the specimens, and the subsequent discussion will quantitatively analyze the trap characteristics of different specimens.

B. DC breakdown strength

The DC breakdown strength of the PP specimens is shown in Figure 14. The scale parameter α_s and shape parameter β_s are obtained according to Equation (4), as shown in Table V. The breakdown field strengths of PP-1 and PP-2 are significantly lower than other specimens, and their breakdown field strength data are widely scattered. In addition, the DC breakdown strength increases with the increase in cooling rate, and the breakdown strength of PP-5 with the highest cooling rate is about 232 kV/mm. This indicates that the breakdown strength of PP is enhanced as the spherulite size decreases, which is consistent with the results of the literature [11].

TABLE V
WEIBULL PARAMETERS OF PP SPECIMENS AT DC BREAKDOWN FIELD STRENGTH

Name	Scale parameter α_s	Shape parameter β_s
PP-1	98.5	3.8
PP-2	123.2	4.7
PP-3	191.1	13.7
PP-4	216.2	14.5
PP-5	232.1	8.7

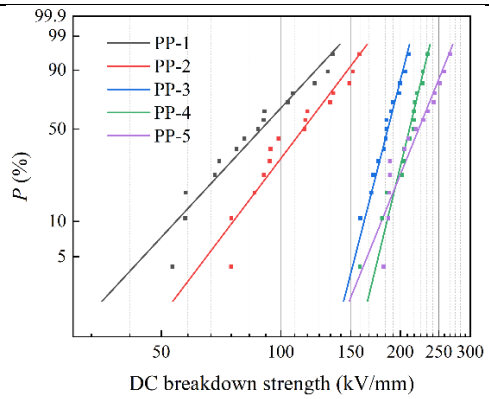

FIGURE 14. **Weibull distribution of PP specimens at DC breakdown strength.**

IV. DISSCUSION

A. EFFECT OF COOLING RATE ON CRYSTALLIZATION MORPHOLOGY

To quantitatively study the effect of cooling rate on the size of spherulites, 100-120 spherulites with clear morphology were selected from PP-1 to PP-5 specimens, respectively. The diameters of these spherulites were measured using

Image J, and the Gaussian distribution curves of the diameters of PP spherulites obtained by fitting the frequency distribution of the diameter data are shown in Figure 15. The spherulite diameter decreases as the cooling rate increases. The dispersion of the spherulite diameter distribution in the PP-1 cooled at 10 °C/min is the largest.

As shown in Figure 16, new nuclei formed near the already formed spherulites as the temperature decreased during the crystallization of PP-1. The appearance of these nuclei indicates that heterogeneous nucleation behavior occurs in PP-1. Heterogeneous nucleation is a process in which molecular chains in the melt are adsorbed to form nuclei around impurities or residual crystals incompletely melted. The appearance of heterogeneous nucleation leads to a large dispersion in the diameter of PP-1 spherulites. The spherulite diameter distributions of PP-2 ~ PP-5 are all more concentrated, proving that the crystallization process is shortened and transformed into homogeneous nucleation due to the elevated cooling rate. Homogeneous nucleation is the process of nucleation by the orderly arrangement of molecular chains formed by the thermal movement of the polymer chain segments in the melt.

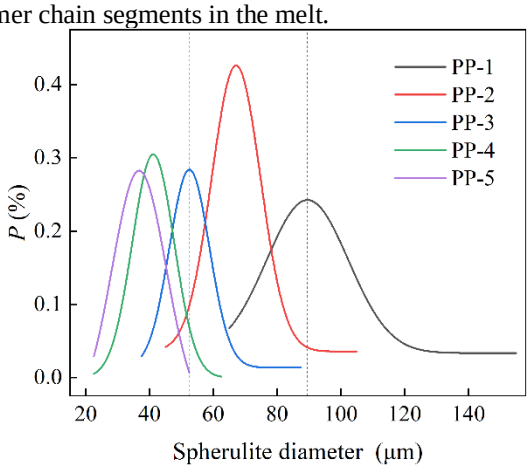

FIGURE 15. Gaussian distribution curve of PP spherulite diameter.

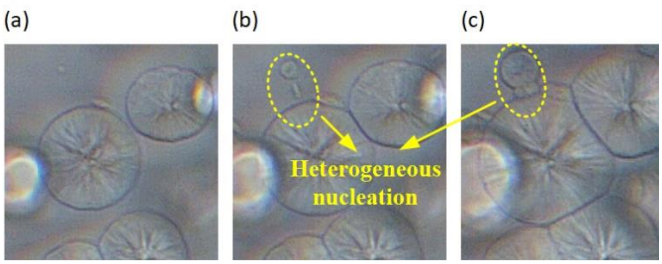

FIGURE 16. Heterogeneous nucleation at 10 °C/min cooling. (a)125.9°C, (b)125.4°C, (c)124.6°C.

In summary, as the cooling rate increases, the nucleation mode transforms from heterogeneous nucleation to homogeneous nucleation, the diameter of spherulites decreases, and the number of spherulites in the same volume increases. Although the rapid cooling leads to decreased spherulites perfection, the spherulites extrusion leads to the restriction of molecular chain activities in the amorphous region, which leads to the increase of density in the amorphous region.

B. EFFECT OF PP CRYSTALLINE MORPHOLOGY ON DC BREAKDOWN STRENGTH

DC breakdown strength of semi-crystalline polymers like PP tends to occur in the weak amorphous region at the interface between the crystalline and amorphous regions [11,23]. This is due to the increased disorder of molecular chains at the interface, where the disordered folding of molecular chains will form carrier traps [24]. The trapping of charges leads to distortion of the electric field, which in turn leads to breakdown. The crystallization of PP in the molten state at different cooling rates will lead to the spherulite formation with different sizes and different degrees of sparsity, which will affect the carrier migration and trap distribution in PP, and the breakdown strength. The mechanism of the influence of the crystalline morphology on the breakdown strength is explained next from two perspectives.

When the applied electric field is low, the conductive current is generated due to the participation of electrons in the conduction band and holes in the valence band in the conductive process, and the carriers migrate mainly in a hopping conductive manner. Ohm's law is satisfied between the conductivity current and the applied field strength at this time. That is, the slope of the fitted curve for each specimen in the low field region in Figure 13f is about 1. As the electric field strength increases, the slope of the fitted straight line increases (>2), indicating the appearance of non-Ohmic conductivity in the high field region. Based on the threshold field strength E_{th} and the quasi-steady-state current density J_{th} at the threshold, the carrier concentration n_f in the conduction band and the carrier mobility μ_f, are obtained as

$$n_f = \frac{9E_{th}\varepsilon_r\varepsilon_0}{8qd} \tag{7}$$

$$\mu_f = \frac{8j_{th}d^3}{9E_t^2\varepsilon_r\varepsilon_0} \tag{8}$$

where ε_r and ε_0 are the relative permittivity and vacuum permittivity of the specimen, respectively; d is the thickness of the specimen; and q is the electronic charge of 1.6×10^{-19} C.

The carrier concentration n_f and carrier mobility μ_f of the PP specimen is shown in Figure 17. As can be seen from Figure 17, the carrier concentration n_f each specimen is in the same order of magnitude. PP-1 has formed more amorphous zones due to slow cooling leading to heterogeneous nucleation involved in the nucleation process and a large dispersion in the distribution of spherulite diameters. This inhomogeneous and sparse structure leads to the easy completion of electron leaps to form carriers. Compared to PP-1, the nucleation mode of PP-2 is transformed and the dispersion of spherulite diameter distribution is significantly smaller. Also, the spherulite diameter of PP-2 is larger compared to PP-3 ~ PP-5. As a result, PP-2 forms a uniform, large, and dense spherulites

structure, which leads to an increase in the energy required for electron leaps, so the carrier concentration is the lowest at about 4.0×10^{17} m^{-3}. When the cooling rate is greater than 20 °C/min, PP-3 ~ PP-5 has a reduced spherulite diameter, decreased perfection and increased n_f due to the faster temperature descent during crystallization. The carrier mobility μ_f of PP-1~PP-4 decreases continuously, with the highest μ_f of about 4.4×10^{-14} $m^2/(V\cdot s)$ for PP-1 and the lowest of about 7.7×10^{-15} $m^2/(V\cdot s)$ for PP-4. It indicates that the diameter of the spherulites decreases as the cooling rate increases, and the confinement imposed on the amorphous region in PP is enhanced and the carrier transport is limited. And the μ_f of PP-5 increases to the level of PP-2, which may be caused by the higher μ_f of PP-5.

In addition to the carrier properties, the crystalline morphology significantly affects the trap properties in PP. The depolarization process of space charge can reflect the trap information. As the depolarization time increases, the charge inside the specimen gradually dissipates, and the average charge density $\rho_s(t)$ inside the specimen can be expressed as:

$$\rho_s(t)=\frac{1}{d}\int_0^d\left|\rho(x,t)\right|dx \tag{9}$$

where d is the thickness of the specimen; $\rho_s(x, t)$ is the charge density at the thickness x at the moment t.

The average charge density during depolarization decays approximately according to the exponential law,

$$\rho_s=Ae^{-t/\tau}+B \tag{10}$$

where A is the initial charge density; B is the residual charge density; and τ is the decay time constant.

Assuming that the charge does not trap again after being trapped, the trap energy level E_t and the trap density $N(E_t)$ can be obtained as:

$$E_t=k_BT_{test}\ln(vt) \tag{11}$$

$$N(E_t)=\frac{Ar't}{d^2qkT\tau f_0(E_t)}e^{-t/\tau} \tag{12}$$

where k_B is the Boltzmann constant, 8.568 × 10-5eV/K; T_{test} is the test temperature, taken as 293.15 K; v is the electron vibration frequency, taken as 3×10^{12} s^{-1}; r' is the mean charge center of mass, taken as 120 pm [25].

The E_t of different specimens after polarization at an electric field strength of 40 kV/mm were obtained according to Equations (10)~(12), as shown in Figure 18. It can be seen that $N_t(E_t)$ increases and then decreases with the increase in cooling rate, and E_t decreases and then increases. It means that the trap becomes shallow and then deep with the increase in cooling rate. Many studies have shown that the increased depth of traps helps to increase the breakdown strength [26]. Due to the weakened molecular chain order, carrier traps are formed at the interface between the crystalline and the amorphous region in PP. When carriers migrate at the interface, the trapping and detrapping of carrier significantly affect the PP insulation properties.

From the analysis on the effect of cooling rate on crystallization morphology, it can be concluded that as the cooling rate changes from slow to fast, the spherulite diameter becomes smaller, the number of spherulites increases, the degree of spherulites perfection gradually decreases, and the bondage in the amorphous region is enhanced. The behavior of carriers appearing in PP such as injection, migration, trapping and detrapping is affected by the crystalline morphology. Figure 19 shows a schematic diagram of the effect of crystalline morphology on the carrier transport properties and trap depth.

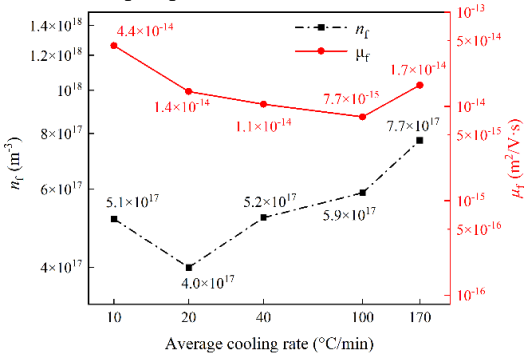

FIGURE 17. **Carrier concentration and carrier mobility**

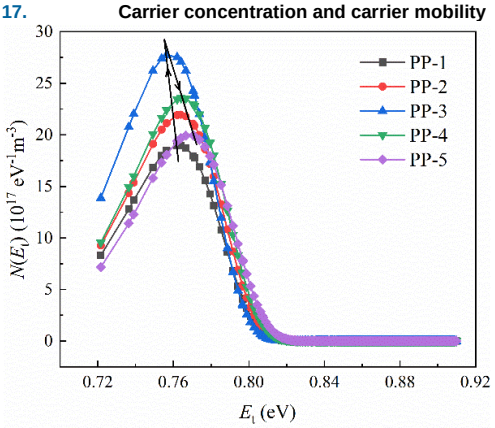

FIGURE 18. **Trap distribution of different specimens**

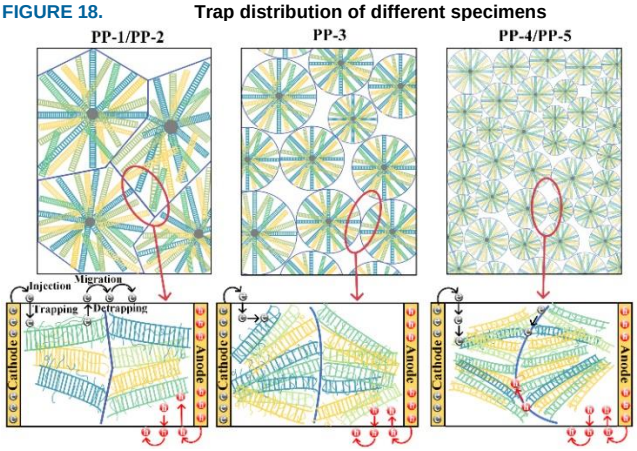

FIGURE 19. **Schematic diagram of the effect of spherulites morphology on trap depth, carrier transport behavior and degree of electric field distortion**

V. CONCLUSION

This article prepared PP specimens with different spherulites diameters by controlling the cooling rate. Based on the test results, the influence of crystal morphology on the physicochemical properties, polarization current, and DC breakdown strength of PP was analyzed, and the following main conclusions were drawn:

1) As the cooling rate increases, the nucleation mode of PP gradually transitions from heterogeneous nucleation to homogeneous nucleation, and the crystallinity first increases and then decreases.
2) As the cooling rate increases, the diameter of the spherulites continues to decrease, the boundaries of the spherulites gradually become blurred, the degree of perfection of the spherulites gradually decreases, and the number of spherulites within the same volume increases. The mutual compression between spherulites leads to an increasing binding on the amorphous region, and the density of the amorphous region increases. At the same time, the reduction in the size of the spherulites facilitates the enhancement of the toughness of the material.
3) The crystalline morphology significantly affects the transport characteristics of carriers. During slow cooling, the interface formed by the dense spherical structure increases the potential barrier for electrons to transition from valence band to conduction band, resulting in lower carrier concentration during slow cooling. As the cooling rate increases, the carriers concentration increases. However, due to the increase in the density of the amorphous region, deep traps are introduced, which limits the transport of charge carriers, effectively reducing electric field distortion and improving DC breakdown strength.

APPENDIX A
COOLING RATE CALCULATION

There is an explanation of the cooling rate calculation. In section 2.1, the average mold cooling rate was used as the specimen cooling rate. Actually, there is an error between the mold temperature and the PP temperature during the cooling process. As shown in Figure 20, with a maximum temperature difference of about 18°C during slower cooling and about 8°C during faster cooling, but the temperature change rate of the mold and the specimen is the same. If the temperature of the specimen is measured directly, it will result in the thermocouple insulation layer melting into the PP during hot pressing. So this paper determines the mold temperature to ensure the purity of the specimen.

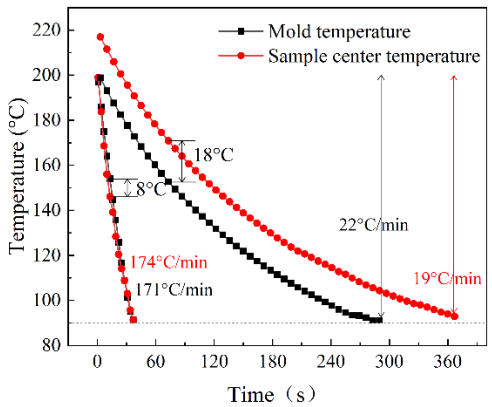

FIGURE 20 Difference between mold temperature and PP temperature.

REFERENCES

[1] J. Su, B. Du, J. Li and Z. Li, "Electrical tree degradation in high-voltage cable insulation: progress and challenges," *High Volt.*, vol. 5, no. 4 353–364, Aug. 2020, 10.1049/hve.2020.0009.
[2] S. Hu., Y. Zhou, C. Yuan, W. Wang, J. Hu, Q. Li and J. He, "Surface-modification effect of MgO nanoparticles on the electrical properties of polypropylene nanocomposite," *High Volt.*, vol. 5, no. 3, pp. 249–255, Jun. 2020, 10.1049/hve.2019.0159.
[3] A. Kalair, N. Abas and N. Khan, "Comparative study of HVAC and HVDC transmission systems," *Renew. Sust. Energy Rev.* vol. 59, pp. 1653–1675, Jun. 2016, 10.1016/j.rser.2015.12.288.
[4] X. Huang, J. Zhang, P. Jiang and T. Tanaka, "Material progress toward recyclable insulation of power cables part 2: polypropylene-based thermoplastic materials," *IEEE Electr. Insul. M.*, vol. 36, no.1, pp. 8–18, Dec. 2020, 10.1109/MEI.2020.8932973.
[5] Y. Zhou, J. He; J. Hu, X. Huang and P. Jiang, "Evaluation of polypropylene/polyolefin elastomer blends for potential recyclable HVDC cable insulation applications," *IEEE Trans. Dielectr. Electr. Insul.*, vol. 22, no. 2, pp. 673–681, Apr. 2015, 10.1109/TDEI.2015.7076762.
[6] M. Zhou, H.Wang, X. Ren, G. Chen, Y. Luo and F. Yu, "Investigation on effect of semiconducting screen on space charge behaviour of polypropylene–based polymers for HVDC cables," *High Volt.*, vol. 7, no. 5, pp.968–981, Apr. 2022, 10.1049/hve2.12212.
[7] G. Mazzanti, "Issues and challenges for HVDC extruded cable Systems," *Energies*, vol. 21, no. 15, Jul. 2021, 10.3390/en14154504
[8] J. D. Hoffman and R. L. Miller, "Kinetic of crystallization from the melt and chain folding in polyethylene fractions revisited: theory and experiment," *Polymer*, vol. 38, no. 13, pp. 3151–3212, May 1997, 10.1016/S0032-3861(97)00071-2.
[9] B. Du, H. Xu and J. Li, "Effects of mechanical stretching on space charge behaviours of PP/POE blend for HVDC cables," *IEEE Trans. Dielectr. Electr. Insul.* vol. 24, no. 3, pp. 1438–1445, Jun. 2017, 10.1109/TDEI.2017.006116.
[10] B. Dang, J. He, J. Hu and Y. Zhou, "Large improvement in trap level and space charge distribution of polypropylene by enhancing the crystalline − amorphous interface effect in blends," *Polym. Int.*, vol. 65, no. 4, pp. 371–379, Jan. 2016, 10.1002/pi.5063.
[11] S. N. Kolesov, "The influence of morphology on the electric strength of polymer insulation," *IEEE Trans. Electr. Insul.*, vol. EI-15, no. 5, pp. 382-388, Oct. 1980, 10.1109/TEI.1980.298330.
[12] K. Ikezaki, T. Kaneko and Toshio. Sakakibara, "Effect of crystallinity on electrical conduction in polypropylene," *Jpn. J. Appl. Phys.*, vol. 20, no. 3, pp. 609-615, Mar.1981, 10.1143/JJAP.20.609.
[13] F. Zheng, M. Gu, J. Dong, Z. An, Q. Lei and Y. Zhang, "Fast space charge behavior in heat - treated polypropylene films," *J. Appl. Polym. Sci.*, vol. 132, no. 28, pp. Apr. 2015, 10.1002/app.42235.
[14] R. Men, W. Jiang, X. Liu, Z. Lei and J. Song, "Effects of cooling rate on space charge characteristics of polypropylene," *Phys. Scr.* vol. 99, no. 2, Jan. 2024, 10.1088/1402-4896/ad1fb7.

[15] L. Hosier, S. Vaughan, G. Swingler, "An investigation of the potential of polypropylene and its blends for use in recyclable high voltage cable insulation systems," *J. Mater. Sci.*, vol. 46, no. 11, pp. 4058–4070, Feb. 2011, 10.1007/s10853-011-5335-9.

[16] Z. Ran , B. Du, M. Xiao, H. Liu and J. Xing, "Effect of crystallization regulation on the breakdown strength of metallized polypropylene film capacitors," *IEEE Trans. Dielectr. Electr Insul.* vol. 28, no. 1, pp. 175–182, Feb. 2021, 10.1109/tdei.2020.009128.

[17] L. Zhang, Y. Zhang, Y. Zhou, C. Teng, Z. Peng and S. Spinella, "Crystalline modification and its effects on dielectric breakdown strength and space charge behaviour in isotactic polypropylene," *Polymers*, vol. 10, no. 4, pp. 406, Apr. 2018, 10.3390/polym10040406.

[18] Z. Li, F. Dai, Y. Wu and B. Du, "Effect of Crystalline Morphology on Electrical Tree Morphology and Growth Characteristics of PP Insulation: From Mesoscopic to Macroscopic," *IEEE Trans. Dielectr. Electr Insul.* vol. 30, no. 3, pp. 989–996, Jun. 2023, 10.1109/TDEI.2023.3249142.

[19] M. Gahleitner, J. Wolfschwenger, and C. Bachner, "Crystallinity and mechanical properties of PP-homopolymers as influenced by molecular structure and nucleation," *J. Appl. Polym. Sci.*, vol. 61, no. 4, pp. 649–657, Jul. 1996, 10.1002/(SICI)1097-4628(19960725)61:4<649::AID-APP8>3.0.CO;2-L.

[20] C. Zhang, Y. Shangguan and Q. Zheng， "Study on thermal behaviour of impact polypropylene copolymer and its fractions," *J. Appl. Polym. Sci.*, vol. 119, no. 3, pp. 1560–1566, Feb. 2011, 10.1002/APP.32827.

[21] A. Layachi, D. Frihi, H. Satha, R. Seguela and S. Gherib, "Non-isothermal crystallization kinetics of polyamide 66/glass fibers/carbon black composites," *J. Therm Anal. Calorim.*, vol. 124, no. 3, pp. 1319–1329, Feb. 2016, 10.1007/s10973-016-5286-0.

[22] C. Grein, K. Bernreitner and M. Gahleitner. "Potential and limits of dynamic mechanical analysis as a tool for fracture resistance evaluation of isotactic polypropylenes and their polyolefin blends," *J. Appl. Polym. Sci.*, vol. 93, no. 4, pp. 1854–1867, Jun. 2004, 10.1002/app.20606.

[23] Li, S., et al., "Short-term breakdown and long-term failure in nanodielectrics: a review," *IEEE Trans. Dielectr. Electr. Insul.*, vol. 17, no. 5, pp. 1523–1535, Oct. 2010, 10.1109/TDEI.2010.5595554.

[24] Y. Gao, J. Li, G. Chen, T. Han and B. Du, "Compatibility dependent space charge accumulation behavior of polypropylene/elastomer blend for HVDC cable insulation," *IEEE Trans. Dielectr. Electr. Insul.*, vol. 27, no. 3, pp. 947–955, 2020, 10.1109/TDEI.2019.008528.

[25] J. Hao, R. Zou, R. Liao, L. Yang and Q. Liao, "New Method for Shallow and Deep Trap Distribution Analysis in Oil Impregnated Insulation Paper Based on the Space Charge Detrapping," *Energies*. vol. 11, no. 2, pp. 271-287, Jan. 2018, 10.3390/en11020271.

[26] Y. Gao, J. Li, Y. Yuan, S. Huang and B. Du, "Trap distribution and dielectric breakdown of isotactic polypropylene/propylene based elastomer with improved flexibility for DC cable insulation," IEEE Access, vol. 6, pp. 58645–58661, Oct. 2018, 10.1109/ACCESS.2018.2874826.

WEI WANG received the B.Sc. and M.Sc. degrees from the Taiyuan University of Technology, China, in 2012 and 2015, respectively. His research interests include high voltage and insulation technology..